Unprecedented New Crystalline Forms of SnSe in Narrow to Medium Diameter Carbon Nanotubes

Charlotte A. Slade,* Ana M. Sanchez, and Jeremy Sloan*

Department of Physics, University of Warwick, UK

E-mail: charlotte.slade@warwick.ac.uk; j.sloan@warwick.ac.uk

Abstract

We report the observation of four unprecedented new crystalline forms of SnSe, obtained as a result of encapsulation in narrow to medium diameter single-walled carbon nanotubes. Aberration-corrected scanning transmission electron microscopy at 80kV revealed linear, zigzag, helical (i.e. 2 x 1) atomic chains and a new form of encapsulated SnSe. This new form is apparently isostructural to free-standing MoS, MoSe and WSe extreme nanowires etched from the corresponding monolayer dichalcogenides. A structural model has been attained from Annular Dark Field (ADF) images. The experimental imaging agrees well with image simulations produced from models anticipated for the new structural forms.

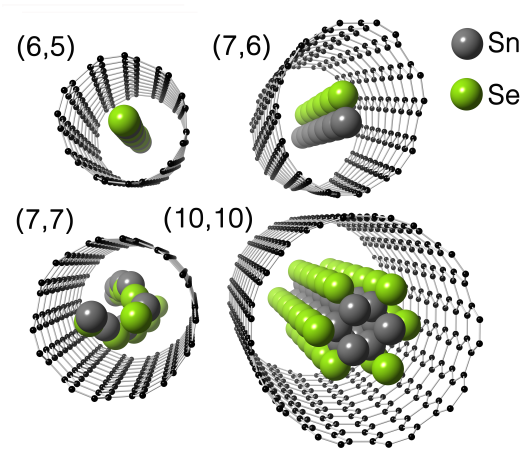

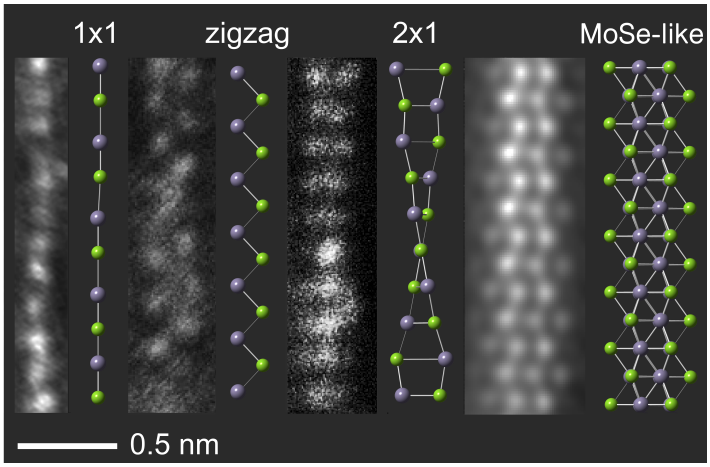

Introduction

Extreme nanowires[1] and encapsulated nanomaterials have recently garnered significant interest, particularly in relation to the use of very narrow Single Walled Carbon Nanotubes (SWCNTs) as confining templates.[2–4] The resulting encapsulation engenders modification to the properties of the host SWCNTs but also profound alteration of the properties of the embedded nanowires, as a consequence of nanostructuring imposed by the latter. The van der Waals forces at the internal surfaces of the SWCNTs constrain the encapsulated material to cross-sections as small as $\simeq$ 1 nm^2, resulting in structures that are completely different to the bulk form of the material,[5,6] producing unprecedented new nanostructured crystalline forms. These can be observed experimentally, but also anticipated by predictive modelling methods including Molecular Dynamics (MD),[7?–9] Density Functional Theory (DFT)[10,11] and *Ab Initio* Random Structure Searching (AIRSS).[12–14] Both experimentation and theoretical modelling are making significant headway in terms of measuring and predicting new functionality of novel nanostructured crystalline forms including modified phonon optics, anticipated band gap modification but, most recently, potentiation of thermoelectric properties in the smallest crystalline forms,[14] prompting new studies into similar materials and other phenomena on a similar scale including electrochemical reactivity.[15]

Additional functionality can be added to these materials when they are prepared and nanoconfined Phase Change Materials (i.e. nC-PCMs). More bulk-like PCMs are already being utilised commercially in optical data storage, although the reversible amorphous-crystalline phase change observed either side of glass transition temperatures on the nanoscale offers promise in memory applications. Nano-confinement takes this premise to the smallest physical scale, as was first demonstrated for nC-GeTe.[16] Additionally, combining the versatile properties of SWCNTs as confining components and the fact that nano-confinement increases both the range of accessible structures for a material and the stability of the encapsulated structures, it is unsurprising the interest that this area of materials science is accumulating. SWCNTs are thermally stable up to temperatures of 1400 K, and can be either metallic

or semi-conducting,[17] and this makes them particularly suitable for investigations into the properties and structural transformation of nC-PCMs. SnSe has many properties that make it suitable as a nC-PCM.[18–21] SnSe melts, and sublimes, congruently from a stoichiometric source material, up to a specific pressure and temperature.[22–26] The size, and form, of the deposited structures is dictated by the diameter of the confining SWCNT (d_{SWCNT}).[27] When calculating the d_{SWCNT} that can accommodate the identified filling structure, the van der Waals radius of carbon ($R_{vdW,C} = 1.77$ Å) must be taken into account.[28] In turn, this total diameter identifies the conformation of the SWCNT, due to the selectivity of the chiral indices.[29,30]

The diameters of the SWCNTs are finite, although spontaneous shrinking and twisting occurs even when the SWCNTs are unfilled.[31,32] Therefore, it is unsurprising that the structures that form can also cause deformations to the SWCNTs.[16] Such deformations can be due to torsion of the confined structure, as is the case of a 2x1 nC-structure and other irregularly distributed nanostructures.[33] Furthermore, as is always the case in nanoscale high-resolution microscopy, but especially in the context of (quasi) 1D materials, it is important to consider the effect of electron beam doses on samples.[34,35] Effects of electron beam irradiation can vary from rotation, or torsion, of the filling material to dissociation of the filling material or the destruction of the SWCNT itself.[36,37]

Prolonged exposure of the filled SWCNTs to the electron beam has also been shown to have potentially beneficial modifying effects on certain nC-fillings, such as amorphisation of Sb_2Te_3 within SWCNTs.[5] Providing the energy of the electron beam is maintained at or below 80 kV, then the filling can be modified without electron beam knock-on damage to the SWCNT. Some extraneous materials in compositional analysis measurements can be attributed to the procedure for synthesising the SWCNTs, which includes the use of Co, Mo, and a supporting catalyst.[38] However, the actual elements present can vary depending upon the SWCNT batch, and the processing of the samples.

We present here a comprehensive study on encapsulation of SnSe in narrower nanotubes

ranging in diameter from $\sim 0.7 - 1.3$ nm. One of the structures encountered is the previously observed 2x2 SnSe form but, in addition to this, we also report that in this diameter range other forms exist including single atomic chain, "zigzag" atomic chains, 2x1 atomic chains and a previously unreported new crystalline form with sixfold symmetry which is apparently isostructural with similar transition metal monochalcogenides (TMC) recently reported for Mo and W formed primarily by etching the corresponding dichalcogenide with an electron beam.[39] This new form of SnSe is the first encapsulated version of these free-standing monochalcogenide MX forms based on a main group metal Sn, as opposed to the transition metals W and Mo.

Results and discussion

Results

The fabrication of SnSe-filled nanotube samples was carried out using Vapour Phase Transport (VPT) via the sublimation method (as described in the Methods section). The purified filled nanotubes were analysed using Aberration Corrected (Scanning) Transmission Electron Microscopy (AC-(S)TEM). High resolution TEM images demonstrated that the sample contained nanotubes in the range of $0.7 - 1.3$ nm, with few outliers. The sensitivity of Annular Dark Field STEM (ADF-STEM) images to the atomic number, Z, allowed the SnSe nanocrystal confined within the SWCNTs to be clearly visualized. Low magnification ADF-STEM images (as shown in Fig. S1) revealed high filling fraction ($\sim 50 - 60$ %) of SWCNTs with SnSe. The existence of external SnSe deposits and structures was observed to be only a minor fraction of the sample following synthesis.

Although ADF imaging is a chemically sensitive technique, the composition of the encapsulated nanocrystal was also determined using Energy Dispersive X-ray (EDX). The EDX analysis of SnSe@SWCNTs bundles routinely gave a Sn/Se ratio of one to one (Sn to Se as 60 ± 1 wt.% to 40 ± 1 wt.%, respectively). Additional EDX investigations of other areas

and SnSe@SWeNT specimens, as well as the VPT remnant material SnSe, gave congruent Sn/Se ratios (i.e. both wt.% and atom %), which confirmed the pursued 1:1 stoichiometric SnSe ratio of the SnSe encapsulated SWCNTs.

Five different structural forms of one-dimensional SnSe nanocrystals were observed over the nanotube diameter range studied. The compiled catalogue of the observed structures of SnSe@SWCNTs, alongside the atomic models for each are shown in Fig. 1. All the structures presented were obtained during the same encapsulation process, using identical fabrication conditions. Therefore, the presence of different SnSe structures would be related to the medium and narrow distribution of CNT diameters. Each structure forms within a characteristic diameter range, so it is possible to order them by the mean diameter of the associated SWCNTs. Line profile measurements of the cubic and new structures show that the SWCNTs that accommodate the new structure are (21 ± 1) % larger than those in which 2x2 cubic SnSe forms. The previously reported 2x2 cubic structure of encapsulated SnSe in narrow SWCNTs was observed both by ADF-STEM and Bright Field STEM (BF-STEM) images (Fig. S2).[33] The catalogue (Fig. 1) also includes 2x1, zig-zag, and linear SnSe atomic chain forms.

When the diameter of the encapsulating SWCNT is $\sim 1.3 - 1.4$ nm, the SnSe filling self-assembles into an unprecedented new crystalline form, which has not been reported to our knowledge (Fig. 2). As mentioned above, the Z sensitivity of ADF-STEM imaging meant that the atomic positions of the nC-SnSe could be clearly viewed, and the contrasting atom intensities analysed. In contrast, the low Z sensitivity afforded in BF-STEM imaging allowed for the carbon walls to be resolved (Fig. 2 BF). Thus, based upon the analysis and measurements of experimental (S)TEM images, an armchair (10,10) SWCNT was considered to be one of the appropriate conformations for initial modelling and image simulation of the new structure (Fig. S3 (a)). This conformation lies firmly within the observed diameter range and the chirality of the SWCNT is such that the confining walls present as continuous lines in experimental images, as opposed to distinct points. Such a SWCNT would be metallic.

However, the observed diameter range for this structure spans a combination of metallic and semiconducting SWCNTs, with the majority being the latter, affording more options to study properties such as changes in conductivity in embedded phase change materials[16] or enhanced thermoelectric characteristics as a result of nanostructuring[15] when these are to be considered.

Fig. 3 corresponds to a ball and stick model of a fragment of the novel SnSe crystalline structure in a tubular SWCNT. Three different views of this structure, corresponding to 30 °, 60 ° and 75 ° rotations around the SWCNT long axis, with respect to a single arbitrary starting view, have been modelled (Fig. 3c). The expanded rotation set over the range $0\ ^\circ - 90\ ^\circ$ has been presented in Fig. S3, which reveals the threefold symmetry of this model, consistent with that reported for 1:1 MX (M=Mo,W; X=S,Se).[40] Although this crystalline form has not been reported previously for SnSe, it should be noted that the above structure is isostructural with a structure observed in monochalcogenide nanowires (MoS, MoSe, and WSe) suspended *in-vacuo*.[39,41] The detailed intensity profile obtained from the ADF-STEM simulated image, corresponding to the 60 ° rotation model, can be clearly correlated with the experimental profile of Fig. 2, as shown in Fig. 4. Thus the modelled structure (Fig. S3) shows good agreement with the experimental data. In addition, the geometrical analysis of bonding in the new structure (Fig. 4 (d)) shows the Sn-Se bond distances to be similar to that observed in bulk (0.272 nm), which is in agreement with previous research on encapsulated SnSe.[33]

We further explored the new SnSe crystalline form analysing the interaction of this structure under beam irradiation. Whilst SWCNTs are only selectively sensitive to electron beam irradiation,[42] the nC-SnSe has been observed to exhibit a variety of behaviours. The most basic of which are for the structure to shift and move inside the SWCNTs. This is more pronounced under prolonged exposure to the electron beam. Such motion can include rotations and translations. An example of a rotation that the nC-SnSe undergoes is depicted in Fig. 3. Whilst this creates challenges in imaging, it offers the valuable opportunity to

be able to study the structure from multiple perspectives, as also reported for the 1:1 MX (M=Mo,W; X=S,Se) monochalcogenide free-standing nanowires. We also note that a new addition to the monochalcogenide family was just reported by Nagata et al., the transition metal telluride MoTe, which is also encapsulated in SWCNTs.[43]

We observed that this structure can rotate inside the SWCNT, thus different projections of the same structure were captured by ADF images in common with similar behaviour noted for the freestanding 1:1 MX free-standing nanowires.[39] *In situ* time sequence experiments, i.e. ADF images recorded at different times (Fig. 3), exposed the deformation of the SnSe filled SWCNTs under the electron beam. The electron irradiation originates the rotation of the crystalline structure inside the SWCNT without destroying it. Three different frames are presented in Fig. 3, corresponding to t= 0 s, 70 s and 135 s. These images correspond to the lattice projection of the novel SnSe crystal. Multislice ADF image simulations of the model at 30 °, 60 ° and 75 ° (using clTEM)[44] are shown next to the experimental images in Fig. 3. The comparison between experimental and simulated images confirmed that these confined structures undergo a crystal rotation inside the SWCNT, under sufficient exposure to the electron beam. These results not only demonstrate the good match between the model and experimental results in different projections, but also the comparative stability of this SnSe atomic structure under the electron beam. This is a clear indication of the good mechanical properties of the SnSe comparable to the findings observed in monochalcogenide MX, which can exhibit both torsional and bending behaviour, according to local beam irradiation conditions.[32,39,40] The rotation of the SnSe inside the SWCNTs allowed analysis to be conducted of multiple views of the structure (Fig. 3). Therefore, we are confident that the simulated TEM and STEM images (Fig. S3 (b) and (c)) are a good match to their experimental counterparts (Fig. 4, S4 and S5).

Under prolonged electron beam irradiation, the nC-SnSe was observed to dissociate (Fig. S6). Therefore, it was important that beam intensity and sample exposure were monitored carefully (~ 2.0 pAcm^{-2} for STEM and ≤ 70.0 pAcm^{-2} for TEM studies), to ensure accu-

rate structural information was obtained. Such behaviour is more likely in single, suspended SnSe@SWCNTs as they will likely be more exposed to the electron beam. Bundles of SWCNTs increase the stability of individual constituent SWCNTs due to the increased support and decreased dose to each SnSe@SWCNT. Furthermore, each structure reacts differently to exposure to the electron beam. The narrower SnSe structural forms are less stable than others and vibrate more when exposed to the electron beam as evident in the single chain, zig-zag chain and 2 x 1 structures presented in Fig. 1(a)-(c) (see also Fig. S6 and S5). The previously reported 2 x 2 form (Fig. 1(d) and S2) and the new form (Fig. 1(e), 3, 4, S4 and S5) are both more robust in the electron beam, but do eventually degrade under either continued electron beam exposure or heightened electron beam dose.

Nanowires, sometimes referred to as Extreme Nanowires,[1] formed at as small as one to three atoms in cross section are being formed by a variety of single elements including S, P, As and Te and, increasingly, from binary systems including CsI, HgTe, KI, SnTe and now SnSe.[10,11,13,14,45–49] In all cases, profound effects are noted in both fundamental changes in crystal growth and phase formation, with polymerization being noted in the case of S, P and As, and continuous chain or coil formation being noted in the case of Te and unprecedented new crystalline single, zig-zag and double zig zag chain forms being reported for semiconductors including SnTe and SnSe. Even between these dramatic low dimensional forms and more conventionally observed bulk-like nanowire forms of these same materials, there exists a size domain in which new crystalline forms are possible, which exhibit novel coordination and novel symmetry and which produce profound changes in physical properties which is true of all of the Extreme Nanowires formed at or below this size domain. For the ultimate scale (i.e. single atomic chain) these including novel metallicity in S,[45] P_4 and As_4 polymerisation,[13,46] realisation of Peierls distortions in Te,[12] and enhancement of the Seebeck coefficient in SnTe.[14] When the atomic thickness reaches 2-3 atoms, novel rod symmetries arise[1,10,11] which give rise to Raman measurable optical phonons that cannot be reproduced in the bulk structure. Similar enhancements to semiconducting band gap,[10,33] and related

improvements to thermoelectric characteristics are also anticipated by theory but in common with several of the characteristics mentioned above, these need to be separated from or incorporated with the properties of the embedding nanotubes. Given the highly selective nature of each structure, with respect to the diameter range of the encapsulating SWCNT, it is possible to obtain a specific form by filtering out the desired chiralities, paying close attention to the conducting form of the host nanotubes.

The discovery of this new form of confined SnSe offers another dimension in the investigation of this compound as a nC-PCM, in contrast to other types of crystalline fillings. These results also form the basis for studies into further nC-PCMs and, in particular, investigations into the variation of the structure of the encapsulated material as a function of the diameter of the NT, and the effect that this has on *in situ* phase changes. These experiments can then be extended to an analysis of further properties of nC-PCMs, such as conductivity. From previous studies,[12,14] enhanced thermoelectric properties would be anticipated, which is the subject of ongoing investigations in this laboratory. Indeed, while mesoscale SnSe nanotubes (180-400 nm in cross-section) have been formed inside alumina templates,[48] theoretical studies by Lin and coworkers predict that forming smaller star-like SnSe nanotubes at a slightly larger scale than our nanostructures theoretical studies by Lin and coworkers predict that forming smaller star-like SnSe nanotubes at a slightly larger scale than our nanostructures (i.e. with an outer diameter of $\sim$2 nm) considerably enhances their thermoelectric performance.[49] Given the conformation options afforded by the confining diameter range of the novel SnSe structure, it is possible to filter out the metal SWCNTs and still be left with a substantial volume of the new structure encapsulated inside semiconducting SWCNTs. Therefore, the margins for investigation into, and application of, the thermoconductive properties of these samples are large.

Methods

Bulk SnSe was vapour phase transported and deposited inside SWCNTs via the sublimation method (Fig. S7).[27] The SWCNTs utilised here have diameters in the range $0.7 - 1.3$ nm: SWCNTs obtained from SWeNT span $0.7 - 1.3$ nm, with few outliers. Prior to filling, 50 mg quantities of the CNT samples were pre-oxidised at ~ 750 K in a tube furnace in air. A ~ 70 mg sample of SnSe (Sigma-Aldrich, now Merck, 99.995 %) was loaded into the end of one half a sublimation 20 cm (14 mm diameter) double ampoule with the pre-oxidised SWCNTs being placed near the central constriction in the second half. The ampoule was sealed under a partial vacuum (0.001 Torr) and the end of the ampoule containing the SnSe was placed in the centre of a 0.3 m long tube furnace heated to ~ 1090 K at a rate of 20 Kmin^{-1}. The SnSe was then allowed to sublime into the other half of the ampoule, following a temperature gradient of ~ 40 K. After 24h, the ampoule was brought back to room temperature at a natural cooling rate.

The SnSe@SWCNT samples were then dispersed in ethanol, using a sonicator, and deposited onto lacey carbon copper TEM grids for analysis. JEOL ARM-200F was used to obtain ADF-STEM (detector angle range 45 mrad-150 mrad) and BF-STEM (detector angle range 0 mrad-23 mrad) images at an electron accelerating voltage of 80 kV, with an electron density of ~ 1.0 nAnm^{-2}. Beam current density was approximated from the read-out on the viewing screen.

Structural models were built in CrystalMaker 9. The conformations, and other properties, of the SWCNTs, and those that would be appropriate for each of the nC-SnSe structures, were obtained via direct line-profile measurements of the respective SnSe@SWCNTs. These were then cross-referenced with calculations of the total size of the nC-SnSe structures, where the total size is comprised of the diameter of the nC-SnSe structure plus two $R_{vdW,C}$. The OpenCL source accelerated multislice simulation software, clTEM, was then utilised in order to obtain the simulated TEM and STEM images from the models.[44,50]

Supporting Information Available

Additional low-resolution STEM images showing high fraction filling in the SnSe@SWCNT samples; ADF- and BF-STEM images of cubic nC-SnSe; extended rotations of the new structure model and accompanying (S)TEM simulations; electron beam irradiation effects on nC-SnSe; experimental set-up for SnSe@SWCNT growth; additional raw and processed ADF-STEM images of new and 2x1 structures.

Acknowledgement

J.S. is indebted to support from EPSRC grants EP/I033394/1 and EP/R019428/1. C.A.S thanks the University of Warwick for funding and support. We are also indebted to Elena Besley and Anton Nizovtsev in Nottingham and also David Quigley and Adrij Vasylenko in Warwick, Andrew Morris in Birmingham and Paulo Medeiros and Jamie Wynn, formerly of Cambridge for insightful discussions.

References

(1) Spencer, J. H.; Nesbitt, J. M.; Trewhitt, H.; Kashtiban, R. J.; Bell, G.; Ivanov, V. G.; Faulques, E.; Sloan, J.; Smith, D. C. *ACS Nano* **2014**, *8*, 9044–52.

(2) Warner, J. H.; Plant, S. R.; Young, N. P.; Porfyrakis, K.; Kirkland, A. I.; Briggs, G. A. D. *ACS Nano* **2011**, *5*, 1410–7.

(3) Warner, J. H.; Ito, Y.; Rümmeli, M. H.; Büchner, B.; Shinohara, H.; Briggs, G. A. D. *ACS Nano* **2009**, *3*, 3037–44.

(4) Wang, Z.; Li, H.; Liu, Z.; Shi, Z.; Lu, J.; Suenaga, K.; Joung, S. K.; Okazaki, T.; Gu, Z.; Zhou, J.; Gao, Z.; Li, G.; Sanvito, S.; Wang, E.; Iijima, S. *J. Am. Chem. Soc.* **2010**, *132*, 13840–7.

(5) Marks, S.; Morawiec, K.; Dluzewski, P.; Kret, S.; Sloan, J. *Acta Phys. Pol. A* **2017**, *131*, 1324–8.

(6) Eliseev, A.; Falaleev, N. S.; Verbitskiy, N. I.; Volykhov, A. A.; Yashina, L. V.; Kumskov, A. S.; Zhigalina, V. G.; Vasiliev, A. L.; Lukashin, A. V.; Sloan, J.; Kiselev, N. A. *Nano Lett.* **2017**, *17*, 805–10.

(7) Wilson, M.; Madden, P. A. *J. Am. Chem. Soc.* **2001**, *123*, 2101–2.

(8) Batra, N. M.; Ashokkumar, A. E.; Smajic, J.; Enyashin, A. N.; Deepak, F. L.; Costa, P. M. *J. Phys. Chem. C* **2018**, *122*, 24967–24976.

(9) Ashokkumar, A. E.; Enyashin, A. N.; Deepak, F. L. *Sci. Rep.* **2018**, *8*, 2–9.

(10) Carter, R.; Sloan, J.; Kirkland, A. I.; Meyer, R. R.; Lindan, P. J. D.; Lin, G.; Green, M. L. H.; Vlandas, A.; Hutchison, J. L.; Harding, J. *Phys. Rev. Lett.* **2006**, *96*, 1–4.

(11) Ivanov, V. G.; Kalashnyk, N.; Sloan, J.; Faulques, E. *Phys. Rev. B* **2018**, *98*, 125429.

(12) Medeiros, P. V.; Marks, S.; Wynn, J. M.; Vasylenko, A.; Ramasse, Q. M.; Quigley, D.; Sloan, J.; Morris, A. J. *ACS Nano* **2017**, *11*, 6178–85.

(13) Hart, M.; White, E. R.; Chen, J.; McGilvery, C. M.; Pickard, C. J.; Michaelides, A.; Sella, A.; Shaffer, M. S.; Salzmann, C. G. *Angew. Chemie - Int. Ed.* **2017**, *56*, 8144–8148.

(14) Vasylenko, A.; Marks, S.; Wynn, J. M.; Medeiros, P. V.; Ramasse, Q. M.; Morris, A. J.; Sloan, J.; Quigley, D. *ACS Nano* **2018**, *12*, 6023–31.

(15) Fu, C.; Oviedo, M. B.; Zhu, Y.; von Wald Cresce, A.; Xu, K.; Li, G.; Itkis, M. E.; Haddon, R. C.; Chi, M.; Han, Y.; Wong, B. M.; Guo, J. *ACS Nano* **2018**, *12*, 9775–84.

(16) Giusca, C. E.; Stolojan, V.; Sloan, J.; Borrnert, F.; Shiozawa, H.; Sader, K.; Rummeli, M. H.; Buchner, B.; Silva, S. R. P. *Nano Lett.* **2013**, *13*, 4020–7.

(17) Sattler, K. D. In *Handbook of Nanophysics: Nanotubes and Nanowires*; Sattler, K. D., Ed.; CRC Press, 2011.

(18) Zhao, L.-D.; Lo, S.-H.; Zhang, Y.; Sun, H.; Tan, G.; Uher, C.; Wolverton, C.; Dravid, V. P.; Kanatzidis, M. G. *Nature* **2014**, *508*, 373–377.

(19) Maier, H.; Daniel, D. R. *J. Electron. Mater.* **1977**, *6*, 693–704.

(20) Shi, W.; Gao, M.; Wei, J.; Gao, J.; Fan, C.; Ashalley, E.; Li, H.; Wang, Z. *Adv. Sci.* **2018**, *1700602*, 1–22.

(21) Yu, J. G.; Yue, a. S.; Stafsudd, O. M. *J. Cryst. Growth* **1981**, *54*, 248–52.

(22) Boone, S.; Kleppa, O. J. *Thermochim. Acta* **1992**, *197*, 109–21.

(23) Zhao, S.; Wang, H.; Zhou, Y.; Liao, L.; Jiang, Y.; Yang, X.; Chen, G.; Lin, M.; Wang, Y.; Peng, H.; Liu, Z. *Nano Res.* **2015**, *8*, 288–95.

(24) Feutelais, Y.; Majid, M.; Legendre, B.; Frics, S. G. *J. Phase Equilibria* **1996**, *17*, 40–49.

(25) Volodin, V. N.; Burabaeva, N. M.; Trebukhov, S. A. *Russ. J. Phys. Chem. A* **2014**, *88*, 2029–2034.

(26) Sharma, R. C.; Chang, Y. A. *Bull. Alloy Phase Diagrams* **1986**, *7*, 68–72.

(27) Eliseev, A.; Yashina, L.; Kharlamova, M.; Kiselev, N. *Electron. Prop. Carbon Nanotub.*; InTech, 2011; Chapter 8, pp 127–56.

(28) Bondi, A. *J. Phys. Chem.* **1964**, *68*, 441–51.

(29) Reich, S.; Thomsen, C.; Maultzsch, J. *Carbon Nanotubes: Basic Concepts and Physical Properties*; Wiley, 2004.

(30) Fouquet, M.; Bayer, B. C.; Esconjauregui, S.; Blume, R.; Warner, J. H.; Hofmann, S.; Schlögl, R.; Thomsen, C.; Robertson, J. *Phys. Rev. B - Condens. Matter Mater. Phys.* **2012**, *85*, 1–7.

(31) Jakubsky, V.; Perez-Obiol, A. *Phys. Rev. B* **2017**, *95*, 245431.

(32) Koskinen, P. *Phys. Rev. Appl.* **2016**, *6*, 1–9.

(33) Carter, R.; Suyetin, M.; Lister, S.; Dyson, M. A.; Trewhitt, H.; Goel, S.; Liu, Z.; Suenaga, K.; Giusca, C.; Kashtiban, R. J.; Hutchison, J. L.; Dore, J. C.; Bell, G. R.; Bichoutskaia, E.; Sloan, J. *Dalt. Trans.* **2014**, *43*, 7391–9.

(34) Egerton, R. F. *Ultramicroscopy* **2013**, *127*, 100–8.

(35) Egerton, R. F.; Li, P.; Malac, M. *Micron* **2004**, *35*, 399–409.

(36) Kumskov, A. S.; Eliseev, A. A.; Freitag, B.; Kiselev, N. A. *J. Microsc.* **2012**, *248*, 117–9.

(37) Jiang, N.; Spence, J. C. *Ultramicroscopy* **2012**, *113*, 77–82.

(38) Kitiyanan, B.; Alvarez, W.; Harwell, J.; Resasco, D. *Chem. Phys. Lett.* **2000**, *317*, 497–503.

(39) Lin, J. et al. *Nat. Nanotechnol.* **2014**, *9*, 436–42.

(40) Lin, Y.-C.; Dumcenco, D. O.; Huang, Y.-S.; Suenaga, K. *Nat. Nanotechnol.* **2014**, *9*, 391–6.

(41) Koh, A. L.; Wang, S.; Ataca, C.; Grossman, J. C.; Sinclair, R.; Warner, J. H. *Nano Lett.* **2016**, *16*, 1210–1217.

(42) Warner, J. H.; Scha, F.; Zhong, G.; Ru, M. H.; Bu, B.; Robertson, J.; Briggs, G. A. D. *ACS Nano* **2009**, *3*, 1557–63.

(43) Nagata, M.; Shukla, S.; Nakanishi, Y.; Liu, Z.; Lin, Y.-C.; Shiga, T.; Nakamura, Y.; Koyama, T.; Kishida, H.; Inoue, T.; Kanda, N.; Ohno, S.; Sakagawa, Y.; Suenaga, K.; Shinohara, H. *Nano Lett.* **2019**, acs.nanolett.8b05074.

(44) Peters, J. J. P. clTEM - OpenCL accelerated multislice. `https://jjppeters.github.io/clTEM/`.

(45) Fujimori, T.; Morelos-Gómez, A.; Zhu, Z.; Muramatsu, H.; Futamura, R.; Urita, K.; Terrones, M.; Hayashi, T.; Endo, M.; Young Hong, S.; Chul Choi, Y.; Tománek, D.; Kaneko, K. *Nat. Commun.* **2013**, *4*.

(46) Hart, M.; Chen, J.; Michaelides, A.; Sella, A.; Shaffer, M. S. P.; Salzmann, C. G. *Angew. Chemie Int. Ed.* **2018**, *57*, 11649–11653.

(47) Senga, R.; Komsa, H.-P.; Liu, Z.; Hirose-Takai, K.; Krasheninnikov, A. V.; Suenaga, K. *Nat. Mater.* **2014**, *13*, 1050–4.

(48) Zhao, L.; Yosef, M.; Steinhart, M.; Göring, P.; Hofmeister, H.; Gösele, U.; Schlecht, S. *Angew. Chemie Int. Ed.* **2006**, *45*, 311–5.

(49) Lin, C.; Cheng, W.; Guo, Z.; Chai, G.; Zhang, H. *Phys. Chem. Chem. Phys.* **2017**, *19*, 23247–53.

(50) Dyson, M. A. Advances in Computational Methods for Transmission Electron Microscopy Simulation and Image Processing. Ph.D. thesis, University of Warwick, 2014.

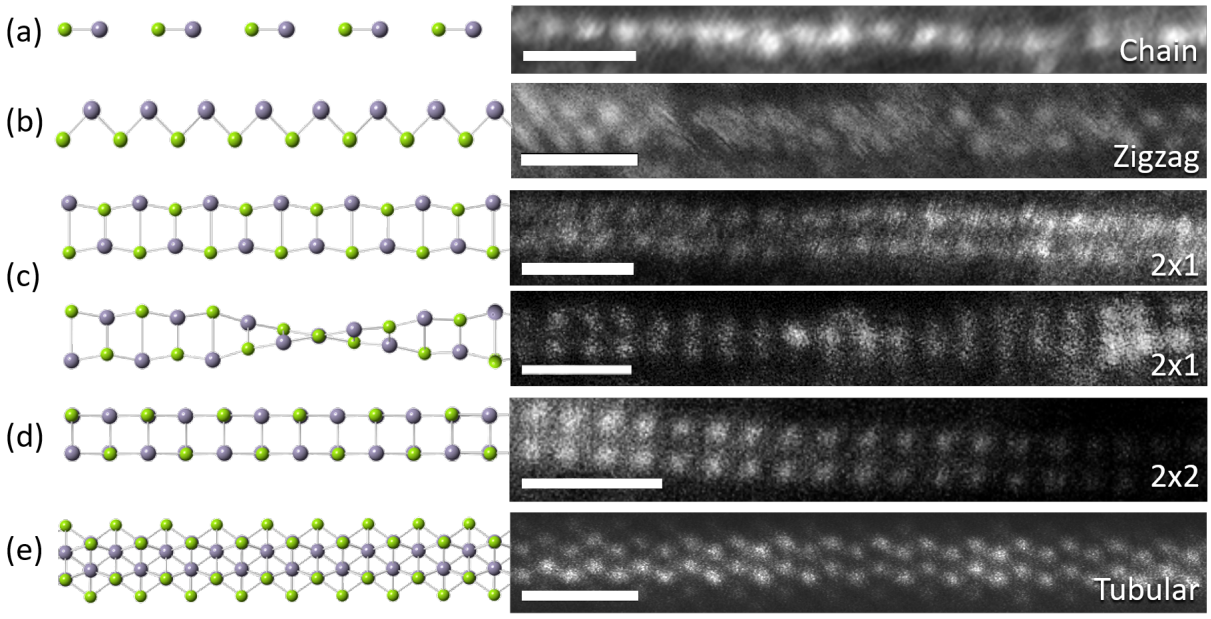

Figure 1: ADF-STEM images of all of the observed forms of encapsulated SnSe nanowires inside SWCNTs, alongside their structural models. The structures are ordered by the mean diameter in which they form. (a) Linear dipole chain. (b) Zig-zag. (c) 2x1. (d) 2x2 cubic. (e) New tubular structure. Scale bars are 1 nm.

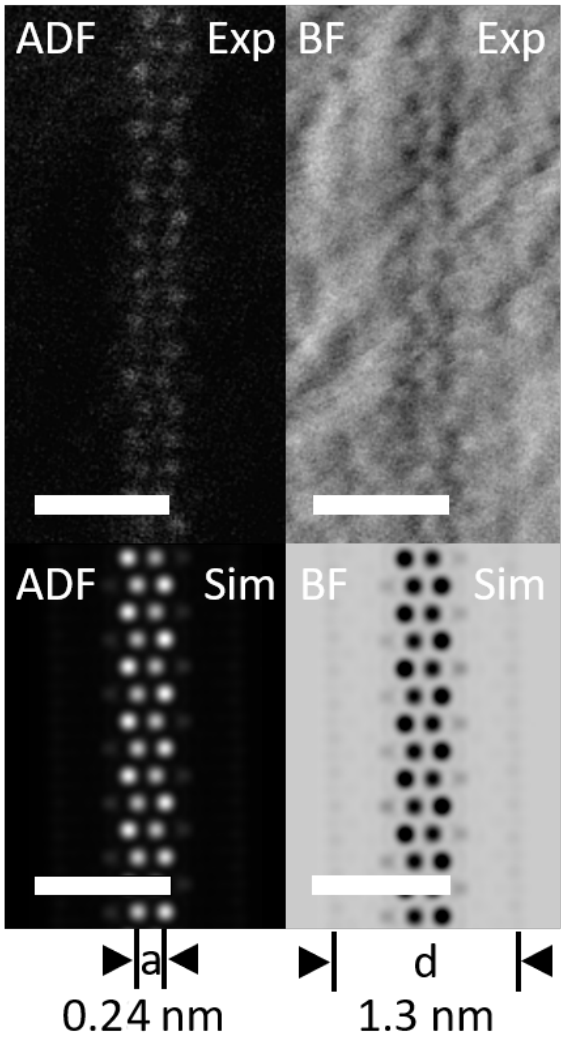

Figure 2: ADF and BF-STEM images of the newly observed form of nC-SnSe, alongside the simulated counterparts. The simulated images were produced from a SnSe fragment inside a (10,10) SWCNT. The indicated measurements are for the diameter of the confining SWCNT, d, and the atomic separation of the SnSe, a, which are concurrent for the experimental and simulated images. Scale bars are 1 nm.

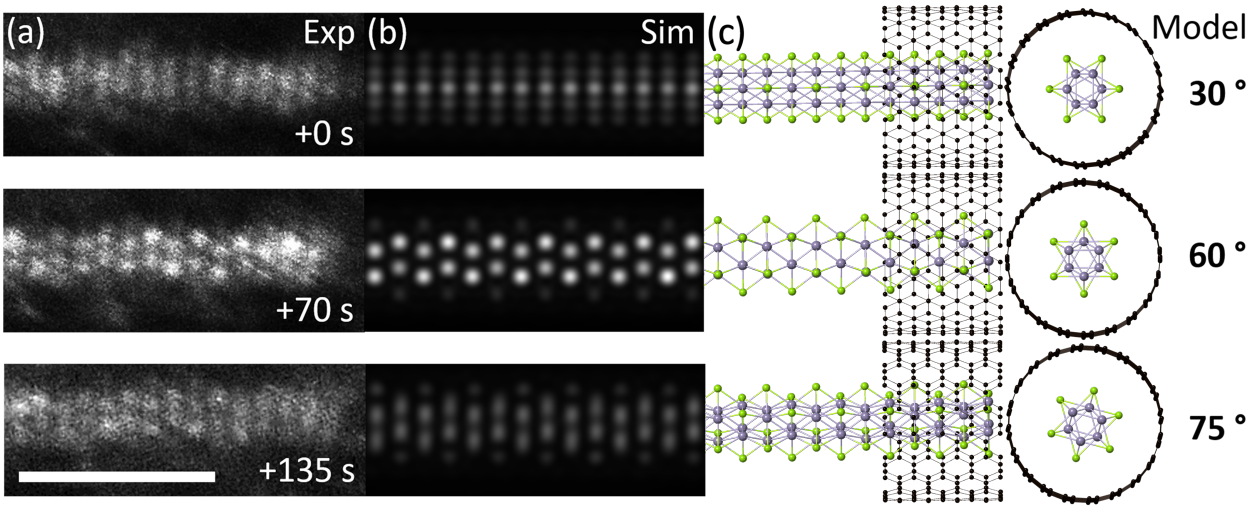

Figure 3: ADF-STEM images of the novel SnSe structure, taken at the indicated time intervals. These are shown alongside the corresponding rotations of the proposed model and their simulated STEM images. Scale bars are 2 nm.

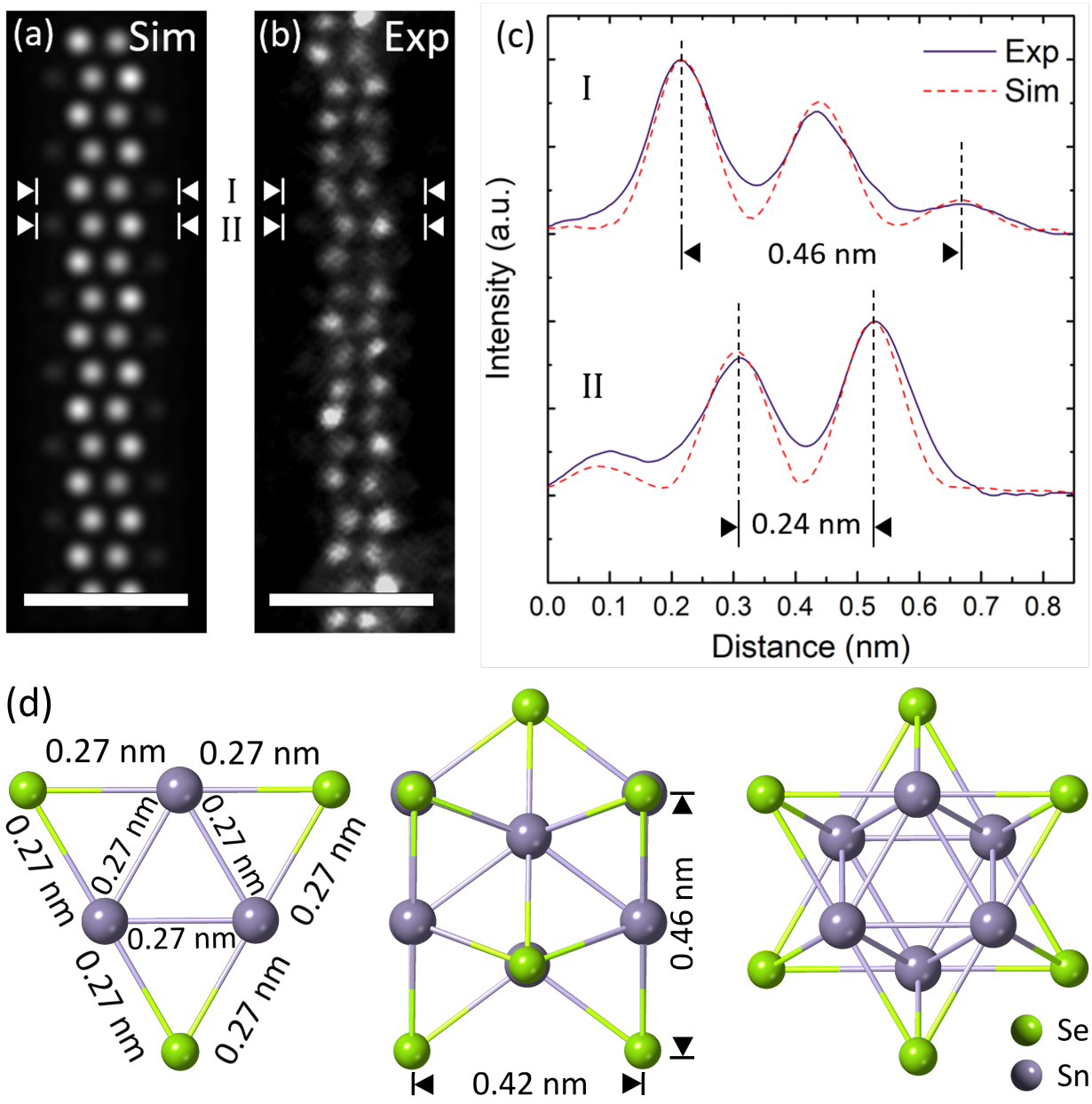

Figure 4: Direct comparison of the (a) simulated and (b) experimental ADF-STEM images of the novel form of nC-SnSe via the corresponding (c) line profile intensities. The experimental line profile intensities are averages across the sum of the equivalent layers. Scale bars are 1 nm. (d) Bond analysis of the model built from experimental data.

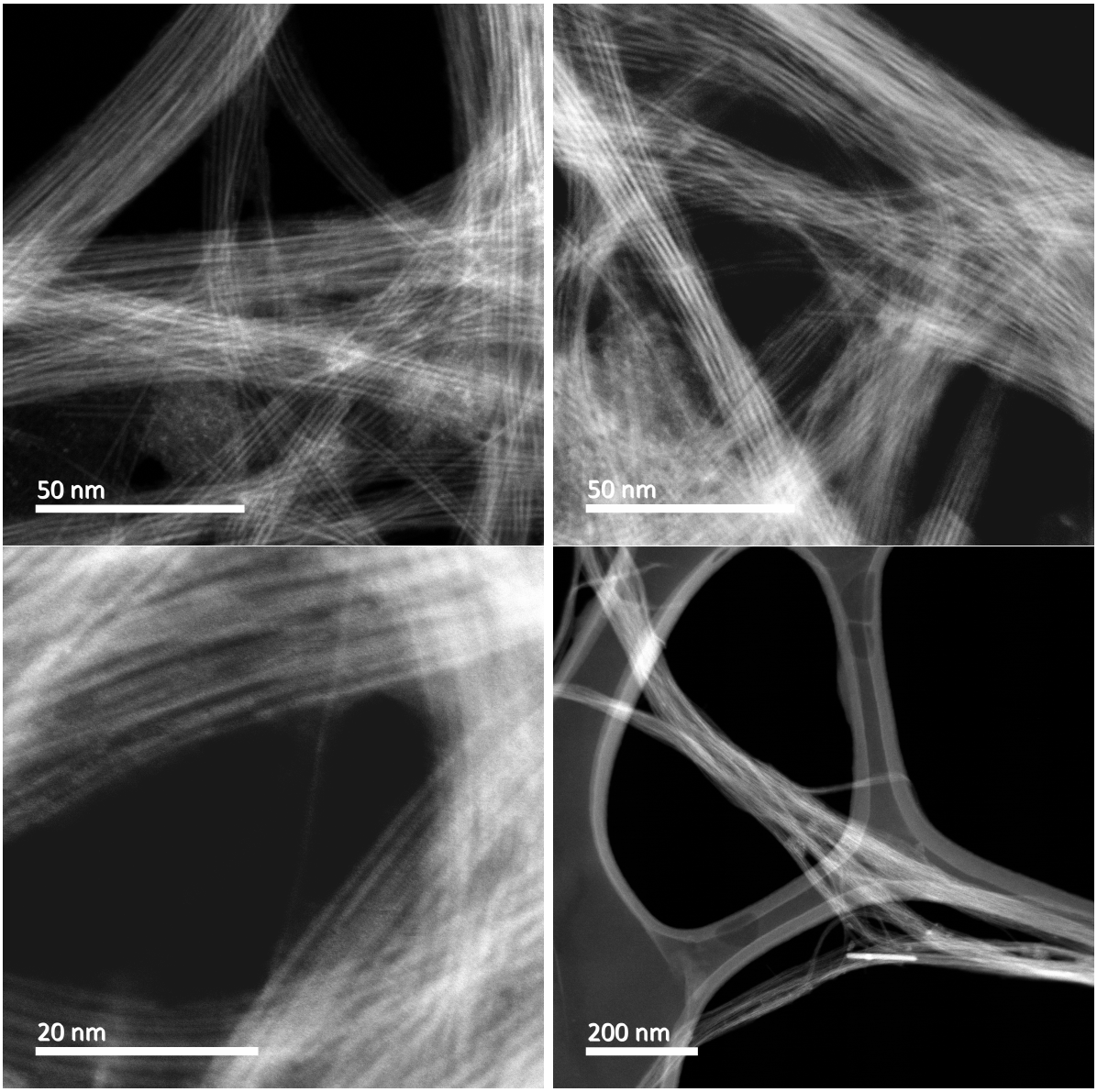

Figure S1: Representative low-resolution ADF-STEM images of the SnSe@SWCNT sample. The prevalence of the ordered, high contrast areas in the images is evidence of quantitative filling of the SWCNTs.

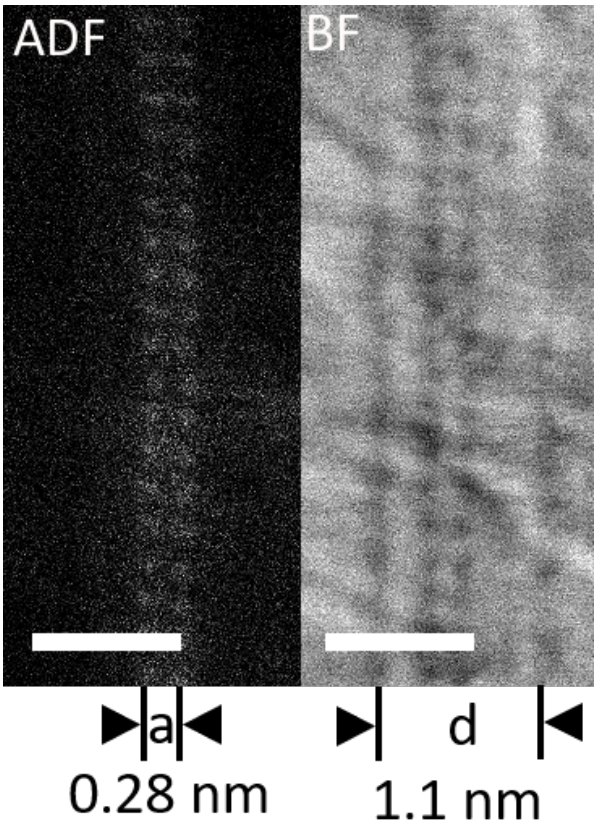

Figure S2: ADF and BF-STEM images of the cubic form of nC-SnSe, with measurements of the diameter of the confining SWCNT, d, and the atomic separation of the SnSe, a. Scale bars are 1 nm.

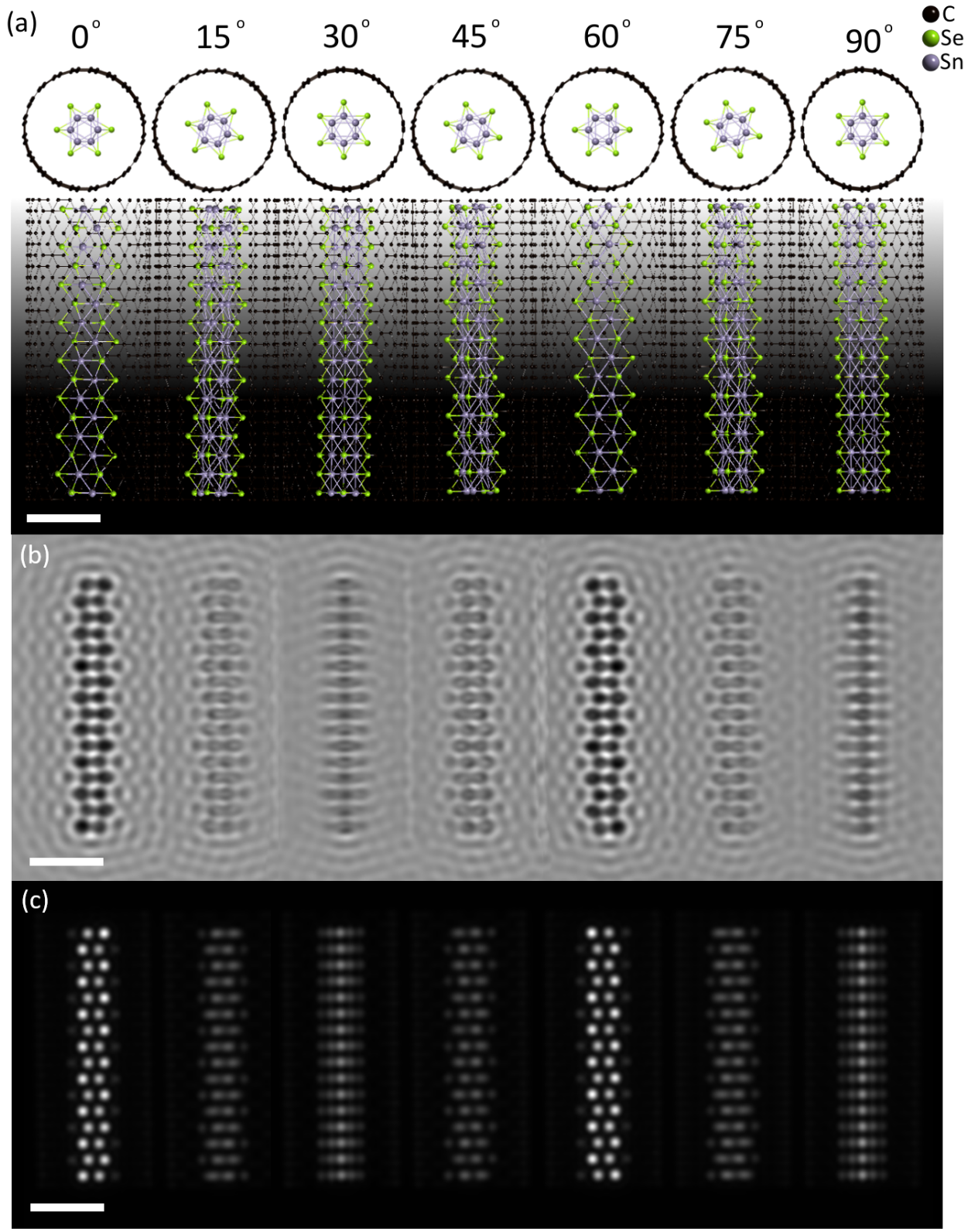

Figure S3: The proposed model inside a (10,10) SWCNT (a) is shown at the rotational intervals of 15 °, from 0 ° to 90 °.These produce observable views of the structure in (S)TEM images. The TEM (b) and ADF-STEM (c) simulations corresponding to the model at these rotations. Scale bars are 1 nm.

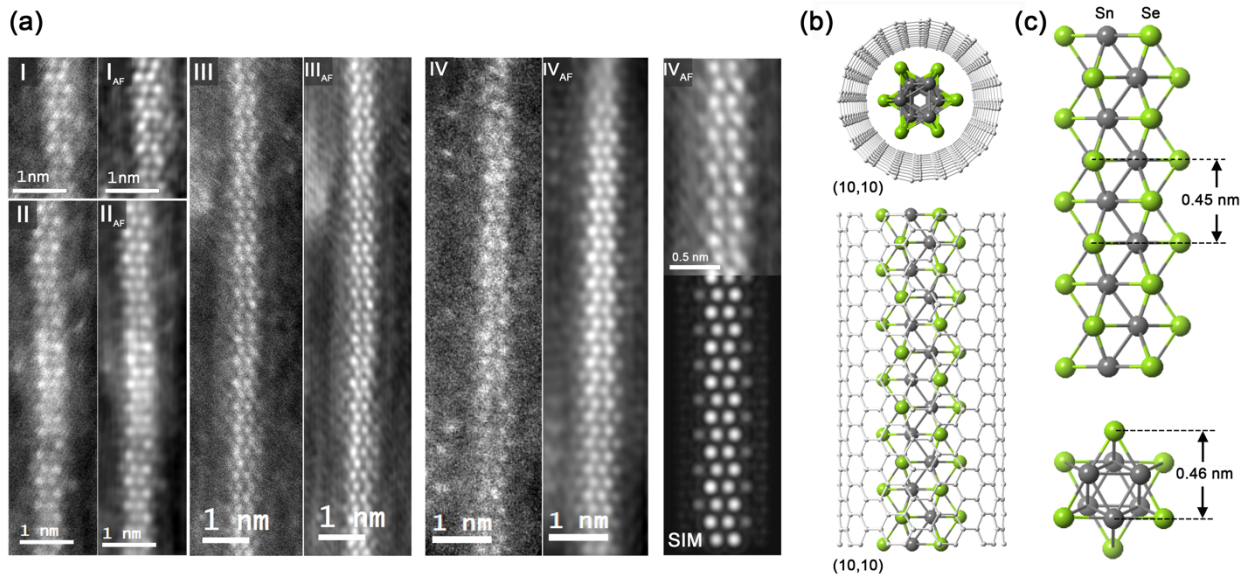

Figure S4: (a) Additional ADF images of MoSe-like SnSe stuctures. (I-IV) are raw ADF STEM images and (IAF-IAF) are the same images but with an adaptive filter applied to the spatial frequencies of images I-IV. Images III and IV were obtained from SnSe fragments that were at least 20-22 nm in length, preserving an identical microstructure over the entire length in each case. At right a detail from IVAF is paired with a corresponding simulation conforming to the geometrically optimized SnSe model depicted in (b). (b) Geometrically optimized MoSe-like SnSe nanostructure encapsulated in a (10,10) SWNT. (c) Schematic depiction of freestanding SnSe nanostructure with major repeats indicated based on averaged measurements from all the ADF images.

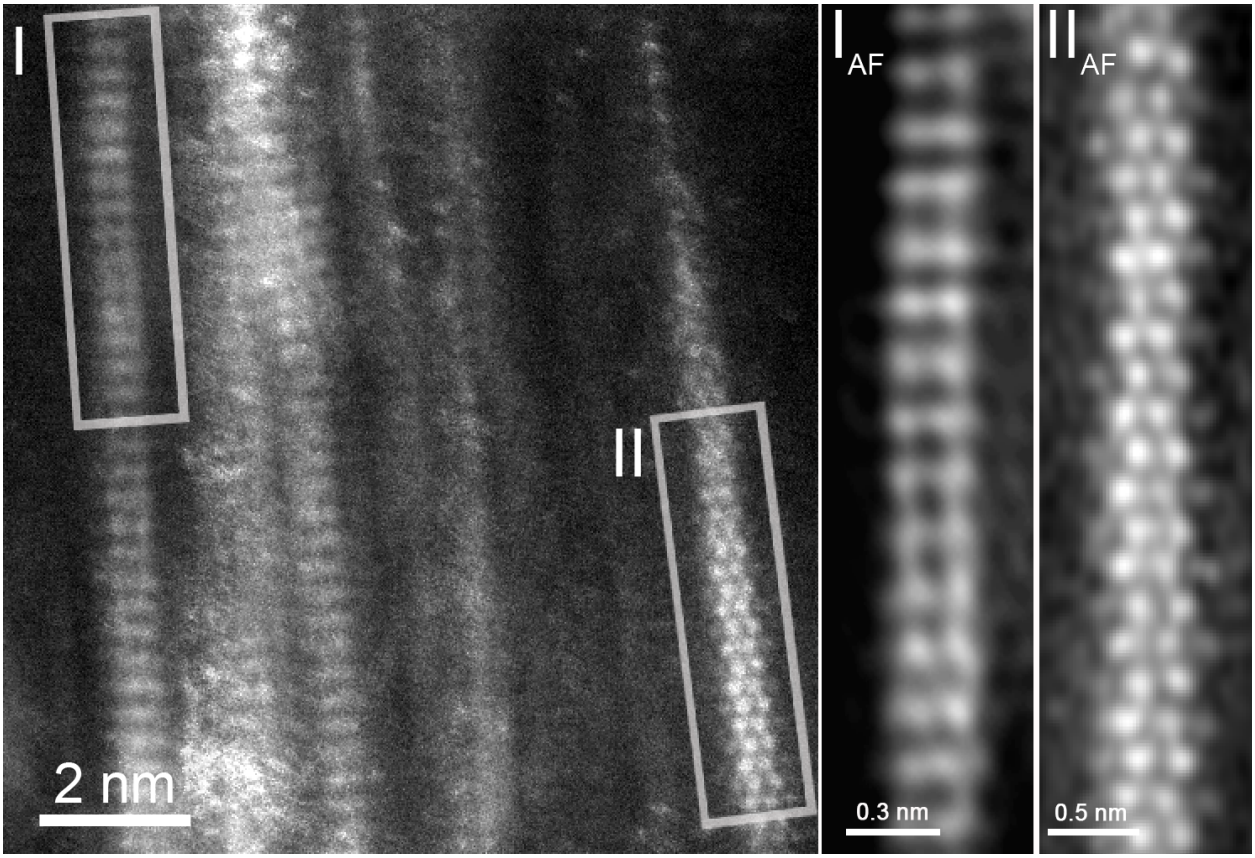

Figure S5: This raw ADF STEM Image shows the co-existence of a 2x1 SnSe fragment (I) with an MoSe-like SnSe nanostructure (II) at right. The indicated details are subjected to adaptive filters in insets IAF and IIAF respectively.

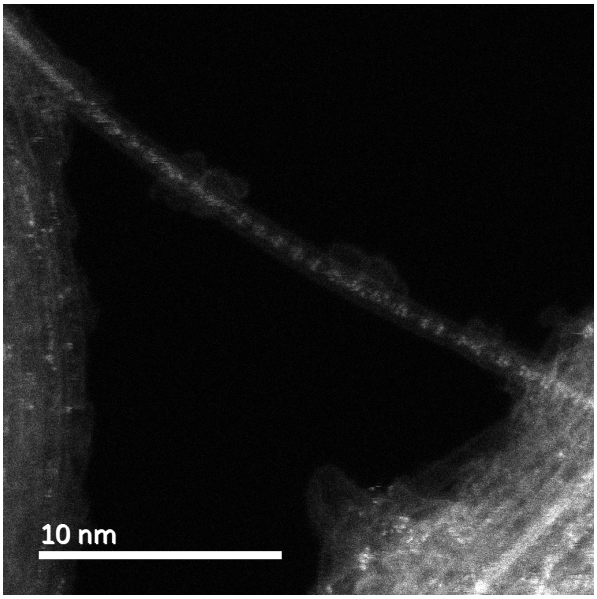

Figure S6: ADF-STEM image of the effect of the electron beam on the encapsulated SnSe. After sufficient exposure to the beam, the filling begins to dissociate into clusters. This image was obtained after a total exposure time of ∼90 s.

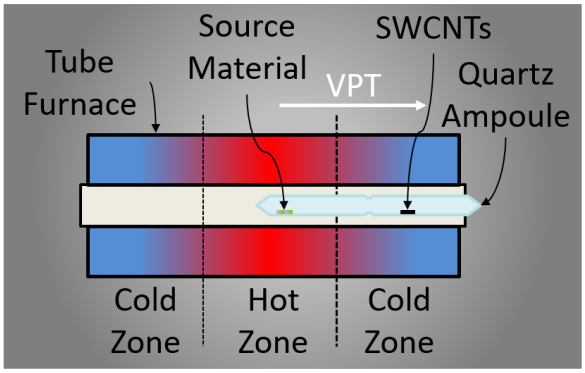

Figure S7: A schematic of the apparatus configuration used for encapsulation of SnSe in SWCNTs via the sublimation method.